Pure appl. geophys. 160 (2003) 2119–2146
0033–4553/03/112119–28
DOI 10.1007/s00024-003-2422-0

Pure and Applied Geophysics

Field Survey and Numerical Simulations: A Review of the 1998 Papua New Guinea Tsunami

PATRICK J. LYNETT,[1] JOSE C. BORRERO,[2] PHILIP L.-F. LIU[3] and COSTAS E. SYNOLAKIS[2]

Abstract—The Papua New Guinea (PNG) tsunami of 1998 is re-examined through a detailed review of the field survey as well as numerous numerical computations. The discussion of the field survey explores a number of possible misinterpretations of the recorded data. The survey data are then employed by a numerical model as a validation tool. A Boussinesq model and a nonlinear shallow water wave (NLSW) model are compared in order to quantify the effect of frequency dispersion on the landslide-generated tsunami. The numerical comparisons indicate that the NLSW model is a poor estimator of offshore wave heights. However, due to what appears to be depth-limited breaking seaward of Sissano spit, both numerical models are in agreement in the prediction of maximum water elevations at the overtopped spit. By comparing three different hot-start initial profiles of the tsunami wave, it is shown that the initial shape and orientation of the tsunami wave is secondary to the initial displaced water mass in regard to prediction of water elevations on the spit. These numerical results indicate that agreement between numerical prediction of runup values with field recorded values at PNG cannot be used to validate either a NLSW tsunami propagation model or a specific landslide tsunami hot-start initial condition. Finally, with the use of traditional tsunami codes, a new interpretation of the PNG runup measurements is presented.

Key words: Submarine landslide, runup, Boussinesq.

1. Introduction

On July 17, 1998 at 08:49 GMT (18:49 local), an earthquake of $M \approx 7$ occurred near the Pacific coast of western Papua New Guinea. Shortly after the earthquake, a destructive tsunami caused extensive damage along the coast from the town of Aitape west to the region around Sissano Lagoon (see Fig. 1). In fact, the death toll was the worst from a tsunami in the past 50 years, with over 1000 persons killed by the tsunami waves. The exact causative mechanism of the tsunami has been the subject of considerable debate, although recently published works (i.e. SYNOLAKIS *et al.*, 2002) strongly indicate a slump source.

[1] Department of Civil Engineering, Texas A&M University, College Station, TX 77843–3136, U.S.A.
[2] School of Engineering, University of Southern California, Los Angeles, CA 90089-2531, U.S.A.
[3] School of Civil and Environmental Engineering, Cornell University, Ithaca, NY 14853, U.S.A.

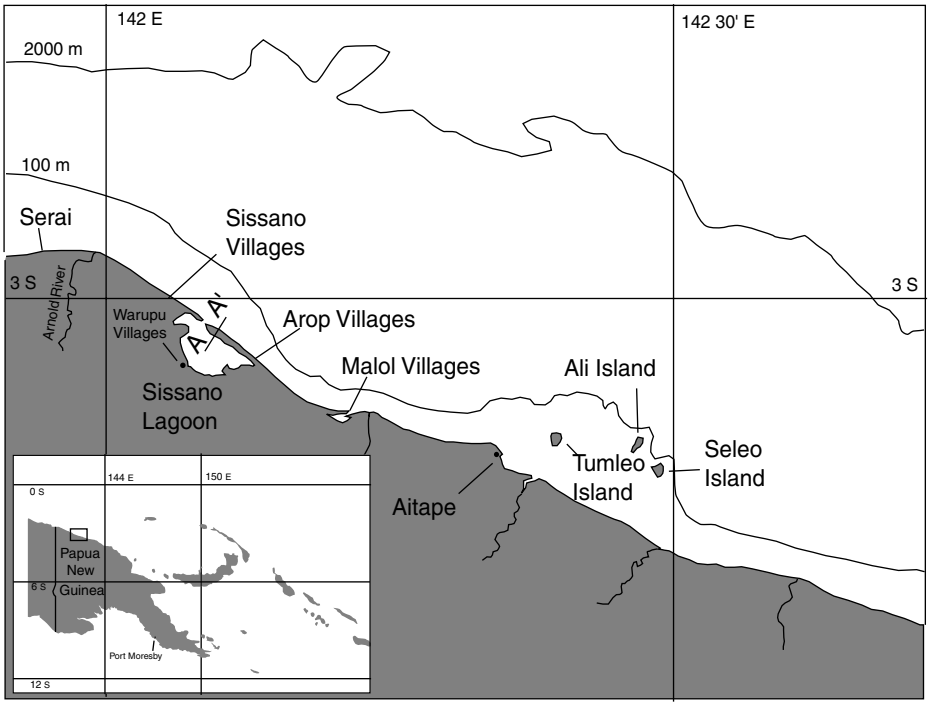

Figure 1
A map of Papua New Guinea and the affected region.

Landslide and slump sources, while poor generators of farfield tsunamis (OKAL, 2003), can generate locally extreme wave heights. Local events are, by definition, caused by tsunamis that cannot transmit energy across large distances, whether it be due to properties of the tsunami wave or a manner of physical boundary. In the case of landslide and slump tsunamis, the deterring factor is a function of the generated wave properties. Typically, a landslide source region encompasses a much smaller area than a dislocation source. Consequently, significantly less total energy is imparted into the water; this energy spreads rapidly and inhibits the possibility of farfield tsunamis. An additional effect of the smaller source region is the generation of a tsunami composed of relatively shorter wavelengths. As the tsunami propagates in the open ocean, the different components will travel at different speeds, opposed to the very long tsunamis of dislocation sources. This dispersion of different frequencies will also act to lessen the amplitude of the tsunami, spreading out energy in the direction of propagation.

Depending on the wavelength of the tsunami, frequency dispersion effects can be important in the nearfield as well, over the distance of a few wavelengths. It will be shown in the numerical section of the paper that this is the case for the PNG tsunami. Additionally, the effect of the initial shape and orientation of the tsunami on offshore

wave heights and wave runup will be analyzed. Lastly, the interpretation of the field data when used in conjunction with a well-studied tsunami code is discussed. First, however, a detailed review of the field survey is presented.

2. Review of Field Survey

2.1 Background

While it is customary during a post tsunami survey to measure the maximum runup and the maximum inundation, in Papua New Guinea the worst damage was concentrated in the region around Sissano Lagoon where measurements of this type were impossible. Sissano Lagoon has the unique feature of a long narrow sand spit between the lagoon and the sea, which has no elevation higher than 3 m and is as narrow as 150 m in some locations. Because of the low relief of the topography and the extremely large wave heights, the sand spit was completely overtopped and water was able to flow over the spit and into the lagoon. Hundreds of villagers lived along the sand bar, and all of their dwellings, canoes and other signs of human habitation were uniformly stripped from the beach.

This fact warrants special care when dealing with measurements taken along the Sissano spit. The data are neither runup nor inundation distances. Since the spit was overtopped and the flow was allowed to propagate across the waters of the lagoon, no true value of "runup" is available. Rather, what we have for this region are measurements of the maximum water elevation, or flow depths when topography is factored in, with the value inferred from local clues such as debris in trees or broken branches up to a certain level.

Despite the trained eyes of the post event field survey team, there is always the possibility of misidentification of a water mark. In terms of broken branches, the surveyor does not know whether it was the tsunami, a big windstorm the week before, or just a dead branch falling from above. Debris in trees also presents problems, as it could have fallen from a taller tree above, or been blown in by the wind or intentionally put there by a former resident (in the case of rags, or buckets).

Within two weeks of the event, the ITST (International Tsunami Survey Team) was mobilized to document the effects along the shore of Papua New Guinea. The team was comprised of participants from Papua New Guinea, Japan, Australia, New Zealand and the United States (KAWATA *et al.*, 1999).

The group split in two with part of the team going by boat along the northern coast from Wewak towards Sissano, and the other half making the journey over land. The boat-based group was able to survey several offshore islands in addition to points along shore (see Fig. 2). The teams met up in Aitape where a relief command center was set up to aid the thousands of victims of the tsunami.

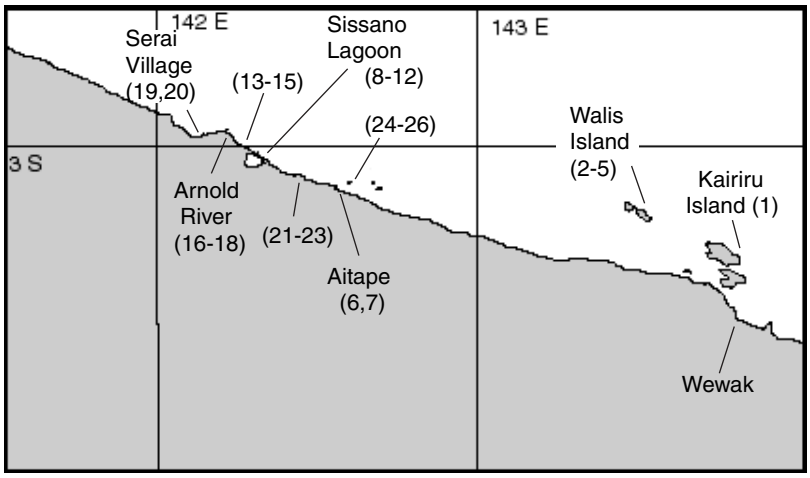

Figure 2
The north coast of Papua New Guinea showing the route taken by the boat-based survey team.

Again the team was split and continued by land and sea towards Sissano. The boat-based team was able to survey as far west as the lumber mill at Serai. The land-based team could only get as far as Malol. However, helicopters were used to ferry the land-based team in the most affected area around Sissano Lagoon.

2.2 Recorded Field Data

The boat-based group was able to obtain twenty-seven measurements on their passage from Wewak to Sissano. Data were taken using standard field surveying procedures which included measuring horizontal inundation, vertical runup and noting possible flow depths through identification of water marks, such as broken branches or debris left in trees.

The following lists all 27 of the points taken by the boat-based team, which included the second and fourth authors. Figure 2 should be referenced to determine the specific location of each of the measurement points.

Site 1 – Purak Village, Kairiru Island

Residents reported feeling the earthquake and noticed a small surge. The runup was up a gentle slope. The uncorrected runup was 1.4 m with an inland penetration of 9.8 m.

Site 2 – Mohu Island, near Walis Island

An uninhabited island. A small log was found above the high tide line along with some other small debris. The log was measured at 1.3 m elevation and 14 m inland penetration along a linear beach slope.

Site 3 – Kameilam Village, Walis Island

Shown this village by locals in a canoe after stopping at Mohu Island. The locals reported having felt the earthquake and hearing the sound of water rushing over the offshore reef. It was probably after dark when the waves affected this area. Maximum runup of 0.3 m with 3.5 m inland penetration.

Site 4,5 – Big Walis Village, Walis Island

Local residents reported feeling the earthquake and hearing the sound of water rushing over an offshore reef. Similar situation as in the previous village. Maximum runup of 0.5 m with 5.5 and 5.2 m inland penetration.

Site 6 – Aitape

Aitape was heavily affected by the earthquake and tsunami. The town was being used as a staging area for the relief effort. This transect had a maximum runup of 3.4 m at a distance of 70 m from shore. The maximum inland penetration was 157 m at an elevation of 2.34 m.

Site 7 – Aitape

This transect had a maximum runup of 3.5 m at a distance of 70 m from shore. The maximum inland penetration was 154 m at an elevation of 1.55 m. This transect crossed over the coast road to a school building. There were erosional features at the base of the school building.

Site 8 – Eastern Spit, Sissano Lagoon

The first transect of the boat team in the devastated area. Flow depths were inferred from broken branches and elevated debris, and measured with a laser distance finder. Water marks were found as high a 9.6 and 10.8 m at distances of 73 and 117 m from shore. This entire area was previously the site of a village. The only remains are the stilts upon which the houses stood. A profile of transect 8 is shown in Figure 3.

Site 9 – Eastern Spit, Sissano Lagoon

Similar to line 8, a profile is shown in Figure 3. This transect is the location of the famous ''bucket in the tree'' photograph. This is the image where a bucket is shown hanging in the small branches of a tree. The branches extend out over the water of the lagoon. The height of this bucket was assumed to be the height of the flow and documented as such in initial reports. The bucket in the tree is show in Figure 4.

Upon further inspection, the authors are not so confident in the bucket as a reliable flow depth indicator. The fact that so many branches remain on the tree is one indicator that such a deep sustained flow did not occur at this location. How the bucket actually got there is still open to debate. Some have suggested that the tree was bent over by the force of the wave and able to pick up debris.

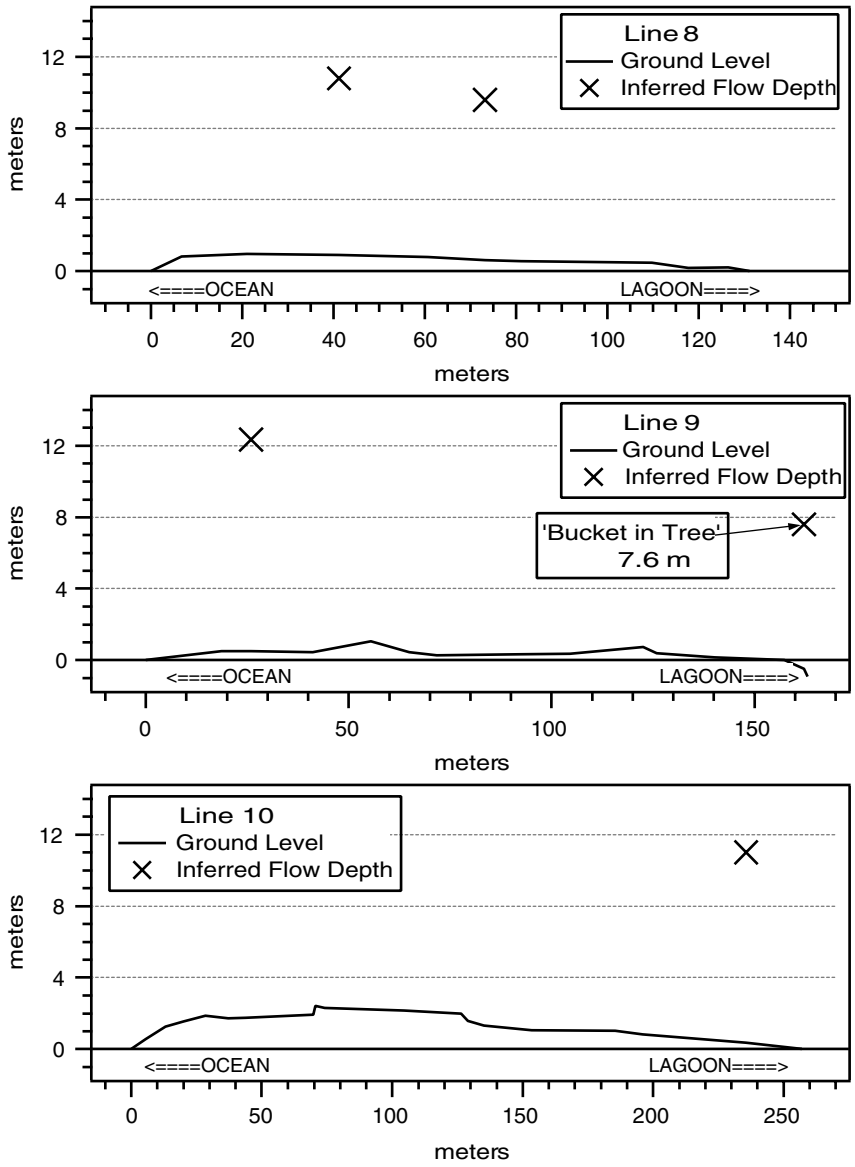

Figure 3
Profiles of line 8, 9, and 10 taken during the 1998 Papua New Guinea tsunami field survey.

Site 10 – Western Spit, Sissano Lagoon

The first transect on the western side of the spit. Numerous houses existed here and were washed away. One potential flow marker was found on this line, a palm frond at 11 m elevation on the back side of the spit near the lagoon.

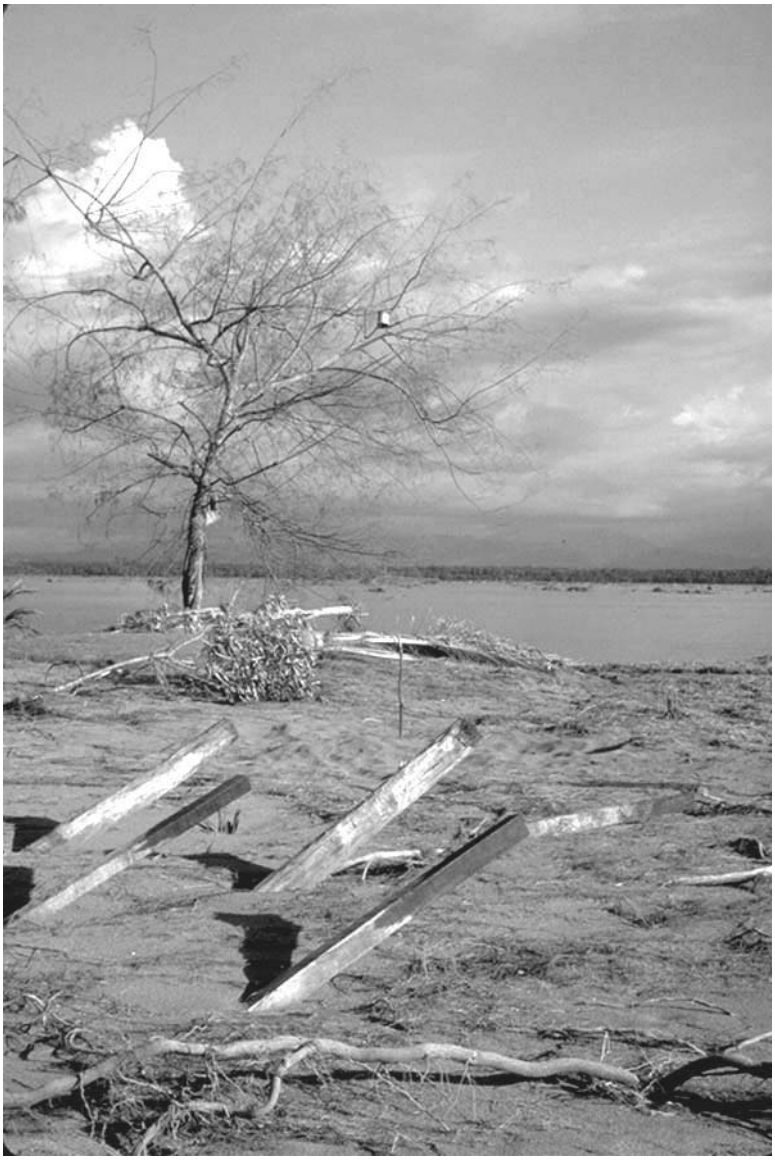

Figure 4
Photo showing house stilts bent back by the force of the wave. A bucket is seen to be hanging from the branches of the tree in the distance. How the bucket got there is still subject to debate.

Site 11 – West of Sissano Village

Near the main village of Sissano. The flow penetrated across a low flat area, and penetrated to the jungle behind the village. We were able to measure up to the edge of the jungle and no further. Debris was piled up at the landward extent of our transect

to a height of 4.6 m above the ground (6.9 m above sea level). The transect of this location is shown in Figure 5.

Site 12 – East of Sissano Village

Near the main village of Sissano, but east of line 11. The tsunami traveled across a low flat area, and penetrated the jungle behind the village. We were able to measure up to the edge of the jungle and no further. Debris was piled up at the landward extent of our transect to a height of 4.5 m above the ground (6.4 m above sea level). This site was the location of a governmental building. The building was a sturdy wooden frame structure built on a concrete foundation. At the time of our survey the building was completely wiped from its foundation. The foundation itself was left with a sand layer up to 9 cm thick. The transect of this location is shown in Figure 5.

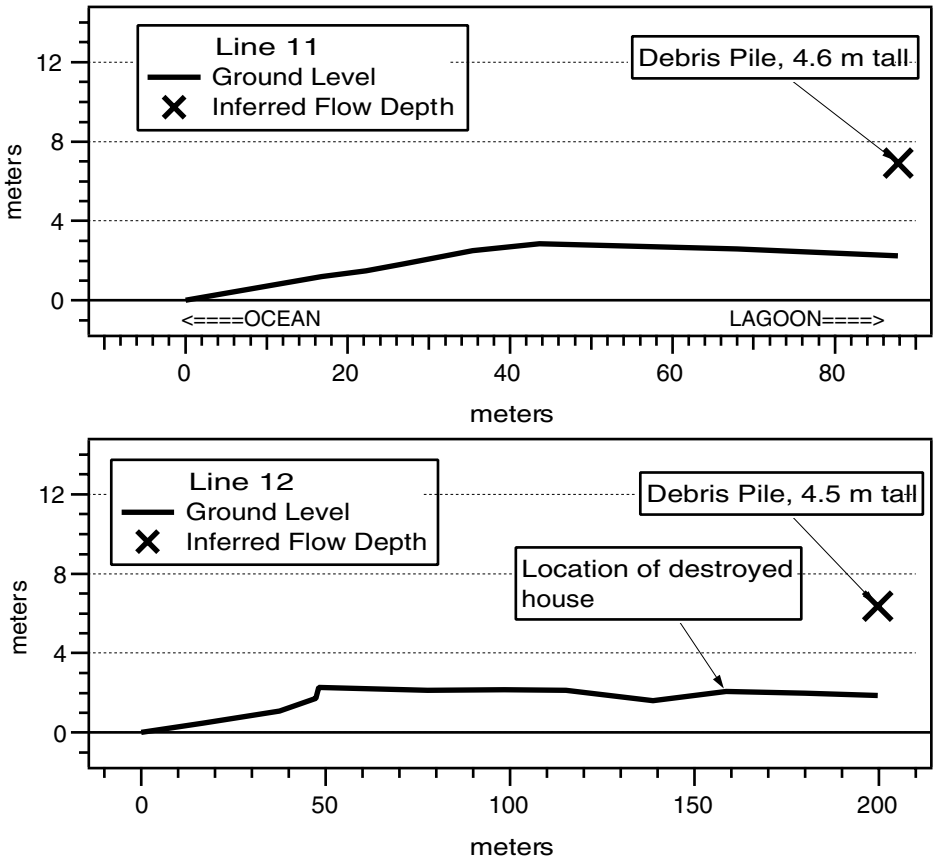

Figure 5
Profiles of lines 11 and 12 taken during the 1998 Papua New Guinea tsunami field survey.

Site 13,14 – Between Sissano and the Arnold River

Measured inland from shore until the jungle became too thick. A debris pile was located 42 m inland. Site 14 was nearly identical, measured 100 m to the west.

Site 15 – East of Arnold River

This transect featured a flow indicator at 3.2 m above ground level a distance of 62 m inland and an elevation of 2.13 m. The maximum inland penetration was 111 m inland at an elevation of 0.5 m above sea level.

Site 16 – Arnold River, East Bank

On the east bank of the Arnold River, a small abandoned village was found. There was a structure near the bank of the river that was partially destroyed by the wave. The structure was built on the river flood plain some 20 m from the river but nearly 100 m from the ocean. The structure was probably damaged by the wave coming in from the river as well as over the beach from the ocean. A suspicious palm frond was noticed hanging from a tree trunk, initially it was believed to be a flow mark, however a local resident informed the team that it was actually a marker placed there by residents to mark private property. Details of the flow characteristics at the mouth of the Arnold River are given in Figure 6.

Site 17 – Arnold River, West Bank

The west bank of the Arnold River was another difficult site to interpret. There were marks of wave uprush, and debris on the floor of the dense forest beyond the tree line. The difficulty in understanding the flow marks was compounded by the location, a river mouth, where unusual focusing and channeling of the flow may have

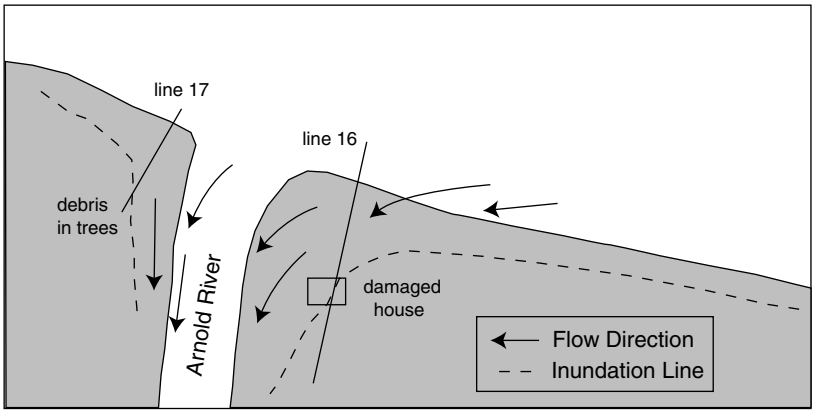

Figure 6
Detail of the inundation measurements at the mouth of the Arnold River.

taken place. A suspicious stick was found in a tree at 5.2 m elevation, but no other similar flow marks were observed. The maximum inland penetration was 86 m to an elevation of 2 m.

Site 18 – West of Arnold River

Continuing west of the Arnold River was a long, relatively straight beach. An unused structure was found 115 m inland beyond the tree line. It was undamaged, but there was a debris line at the foot of the structure. The wave had to overtop a 2.5 m beach crest at 75 m inland before depositing the debris at the structure – 115 m inland, 2.3 m elevation.

Site 19 – Serai Village

Serai Village is approximately 5 km west of the heavily damaged Sissano Villages. However at Serai, there was no damage. The wave did not reach the houses. The water overtopped the berm crest at 3.8 m elevation and 38 m inland. Its maximum excursion was 57 m at an elevation of 3.4 m. It should be noted that the beach in this area is much steeper than at Sissano.

Site 20 – Serai Village

Just west of Serai is the Erkan Log Yard. This is a location where large ships come in to have logs loaded for export. The beach is steep and backed by high steep cliffs. The local residents noted that there were several large rockslides on these cliffs during the earthquake. These rockslides confirmed survey team members in their speculations, developed earlier in the field, that underwater landslides may have triggered the tsunami.

Sites 21,22,23 – Returning to Aitape

These three points were taken along the beach between the Arnold River and Serai. They each gave consistent values of debris in the trees fronting the beach. The heights of the debris above sea level were 7.2, 5.1, and 6.9 m at distances of 29 m, 26 m and 27 m, respectively. Because of a lack of time, the maximum inundation was not found for each of these profiles.

Sites 24,25,26 – Tumleo Island offshore of Aitape

The small Island of Tumleo, approximately 1 km offshore of Aitape was also affected by the tsunami waves. The island has a broad, shallow coral reef surrounding it. Site 23 was at the main village on Tumleo. The wave penetrated a distance of 70 m and maximum runup was 2.4 m. Site 25 was at Ali Village on Tumleo. Runup was 3.7 m with 88 m of inundation. Site 26, the village of Nowom, faced towards the direction of the incoming wave. Runup was 4.2 m and inundation was 96 m.

3. Numerical Modeling of the Tsunami

The extensive field work described in the previous section provides a unique opportunity to achieve an understanding of the atypical source mechanism of this devastating tsunami. Through comparing the numerical runup/flow depth values with those that were recorded by the field team, numerical models can shed light onto the characteristics of the tsunami, which might then provide information of the dynamics of the underwater landslide. Additionally, the field data allows for validation of the numerical models, making them increasingly trustworthy in future simulations.

The tsunami generated by this slump is not the typical tsunami that has been modeled for decades using the nonlinear shallow water (NLSW) equations. These equations are accurate for large scale tsunamis, such as those that impact the entire Pacific rim, whose wavelengths are very large compared to the ocean depth. Local tsunamis, such as at PNG, have wavelengths that are still large compared to the water depth, on the order of 10 times the depth. For waves of this length, the NLSW equations have large, leading order errors. Therefore, it is suspect to use NLSW models to draw conclusions about local tsunami events. On the other hand, the Boussinesq equations are well-known to be accurate for waves of this length.

The Boussinesq equations are derived under the assumption that nonlinearity and frequency dispersion are weak, i.e.,

$$O(\varepsilon) = O(\mu^2) \ll 1, \tag{1}$$

where $\varepsilon =$ wave amplitude/water depth and $\mu =$ water depth/wavelength. The resulting approximate continuity equation, in dimensional form, is

$$\frac{\partial(h+\zeta)}{\partial t} + \nabla\cdot[(h+\zeta)\mathbf{u}_\alpha] - \nabla\cdot\left\{h\left[\left(\frac{h^2}{6} - \frac{1}{2}z_\alpha^2\right)\nabla(\nabla\cdot\mathbf{u}_\alpha) - \left(\frac{h}{2} + z_\alpha\right)\nabla\left(\nabla\cdot(h\mathbf{u}_\alpha) + \frac{\partial h}{\partial t}\right)\right]\right\} = 0. \tag{2}$$

Equation (2) is one of three governing equations for ζ and $\mathbf{u}_\alpha$, the free surface displacement and the depth-integrated horizontal velocity vector. The other two equations come from the horizontal momentum equation, which is given in vector form as

$$\frac{\partial\mathbf{u}_\alpha}{\partial t} + \mathbf{u}_\alpha\cdot\nabla\mathbf{u}_\alpha + g\nabla\zeta + \frac{\partial}{\partial t}\left\{\frac{1}{2}z_\alpha^2\nabla(\nabla\cdot\mathbf{u}_\alpha) + z_\alpha\nabla\left[\nabla\cdot(h\mathbf{u}_\alpha) + \frac{\partial h}{\partial t}\right]\right\} = 0. \tag{3}$$

Equations (2) and (3) are the coupled governing equations, written in terms of $\mathbf{u}_\alpha$ and ζ, for weakly nonlinear, weakly dispersive waves generated by a seafloor movement. This set of equations is most commonly known as the "extended" Boussinesq equations, and will be referred to as "BOUS" in this paper. We note here

that $\mathbf{u}_\alpha$ is evaluated at $z = z_\alpha(x,\ y,\ t)$, which is a function of time. The choice of z_α is made based on the linear dispersion characteristics of the governing equations (e.g., NWOGU 1993; CHEN and LIU, 1995). Assuming a fixed seafloor, in order to extend the applicability of the governing equations to relatively deep water (or a short wave), z_α is recommended to be evaluated as $z_\alpha = -0.53\,\mathrm{h}$. In the following analysis, the same relationship is employed.

Also, a set of model equations can be derived where it is assumed that frequency dispersion is unimportant, i.e.,

$$O(\mu) \ll 1 \tag{4}$$

which yields the well-studied NLSW model:

$$\frac{\partial(h+\zeta)}{\partial t} + \nabla \cdot [(h+\zeta)\mathbf{u}_\alpha] = 0, \tag{5}$$

$$\frac{\partial \mathbf{u}_\alpha}{\partial t} + \mathbf{u}_\alpha \cdot \nabla \mathbf{u}_\alpha + g\nabla\zeta = 0. \tag{6}$$

3.1 Numerical Model

The structure of the current numerical model is described in detail in LYNETT and LIU (2002), where it was employed to model landslide generated waves and runup. The numerical scheme is a high-order predictor-corrector method, employing a third-order in time explicit Adams-Bashforth predictor step, and a fourth-order in time Adams-Moulton implicit corrector step (PRESS *et al.*, 1989). The implicit corrector step must be iterated until a convergence criterion is satisfied. All spatial derivatives are differenced to fourth-order accuracy, yielding a model which is numerically accurate to $(\Delta x)^4, (\Delta y)^4$ in space and $(\Delta t)^4$ in time. Runup, inundation, and overtopping by the tsunami can be examined. The moving boundary scheme employed here is the technique developed by LYNETT *et al.* (2002). Founded around the restrictions of the high-order numerical wave propagation model, the moving boundary scheme utilizes linear extrapolation of free surface and velocity through the shoreline, into the dry region. This approach allows for the five-point finite difference formulas to be applied at all points, even those neighboring dry points, and thus eliminates the need of conditional statements. To simulate the effects of wave breaking, the eddy viscosity model (ZELT, 1991; KENNEDY *et al.*, 2000) is used here. Readers are directed to KENNEDY *et al.* (2000) for a thorough description and validation of the breaking model, and the coefficients and thresholds given therein are used for all the simulations presented in this paper. Both BOUS and NLSW simulations utilize the same numerical algorithm and initial conditions for the simulations to be presented, the only difference being the dispersive, $O(\mu^2)$, terms are not calculated for the NLSW runs.

3.2 Dispersion Effects on Two PNG Initial Conditions

In this section, two of the reported initial conditions for the PNG event, used previously in NLSW models, will be employed in both NLSW and BOUS simulations. These "hot start" initial conditions are meant to yield a reasonable facsimile of the free surface disturbance caused by the slump. Thus, the actual movement of the slump is not being recreated here; rather, a very simplified approach has been taken. The initial free surface condition, with zero velocity, is placed above the slump region and evolves after the numerical simulation is started. These initial conditions are based on a number of observations of the post-slump seafloor profile, as well as assumptions of the failure motion (SYNOLAKIS *et al.*, 2002). Figures 7 and 8 depict the two initial conditions to be examined in this section.

The initial condition in Figure 7, called in this paper the short-fat initial condition, represents the initial condition founded on recent observations of the offshore slump. This condition can then be thought of as more up-to-date than the long-narrow initial condition shown in Figure 8, which had been developed before offshore studies of the slump area had been undertaken. It must be noted that there is a large degree of uncertainty in even the short-fat initial condition, as these initial conditions attempt to approximate a dynamic situation (tsunami generation and seafloor movement occurring simultaneously) with a static, "hot start" initial condition. It is, however, difficult to quantify this error, as little can be inferred of the exact motion of the slump.

For simplicity, the short-fat initial condition will be referred to as SFIC, and the long-narrow initial condition as LNIC. The bathymetry used in these simulations is derived from the bathymetry collected during a post tsunami offshore cruise by the Japanese research vessel Kairei (TAPPIN *et al.*, 1999), and is limited to depths greater than 200 m. For the region between the shoreline and 200 m depths, both linear interpolation and local bathymetric charts were used. Before looking at the numerical output, the expectation of the importance of frequency dispersion effects can be roughly inferred. For both initial conditions, the wavelength is on the order of 10 km in a water depth of about 1.5 km. From linear analysis, it should be expected that initially this wave will behave as an intermediate water depth wave, not a shallow water depth, or long, wave. For reference, the ratio of the wave speed of a 10 km wave to the wave speed of a long wave in 1.5 km of water is 0.9. Thus, initially, frequency dispersion will play an important role. However, as the wave propagates into shallower water, frequency dispersion effects become increasingly minor. The question to be answered is: Will the dispersion effects near the source, in the deeper water, play a significant enough role to alter the waveform in the shallow water? In an attempt to resolve this question, for each of the two initial conditions, simulations were run using both the BOUS (including weak frequency dispersion effects) and NLSW (non-dispersive) models.

First, we examine the LNIC. Figure 9 shows a summary of the numerical results. In the top row of the figure, snapshots of the free surface are taken from both

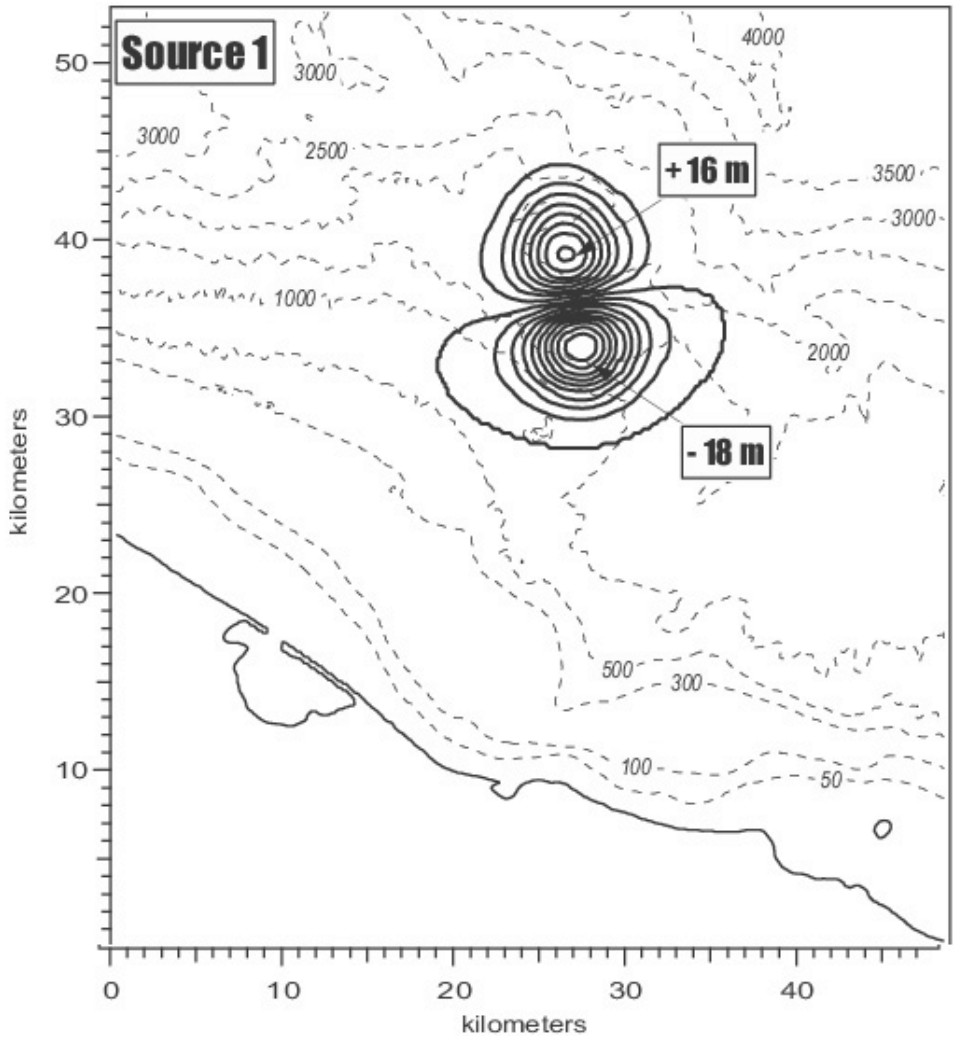

Figure 7
The short-fat initial condition (SFIC) for the Papua New Guinea event. The island is located on the bottom of the figure; Sissano Lagoon is shown.

simulations at a time of 3 minutes after the hot start. Both images show a leading depression wave traveling towards the spit, while a leading elevation wave encroaches upon the shore to the west of the spit. Differences between the two are obvious, with the BOUS simulation exhibiting a well-defined secondary depression wave moving towards the spit. Also, the wave predicted by NLSW at this time has a larger height than that predicted by BOUS. The middle plot in the figure shows the difference in the predicted maximum free surface elevation between the models, where positive values indicate the NLSW predicted a larger free surface elevation at that point. In

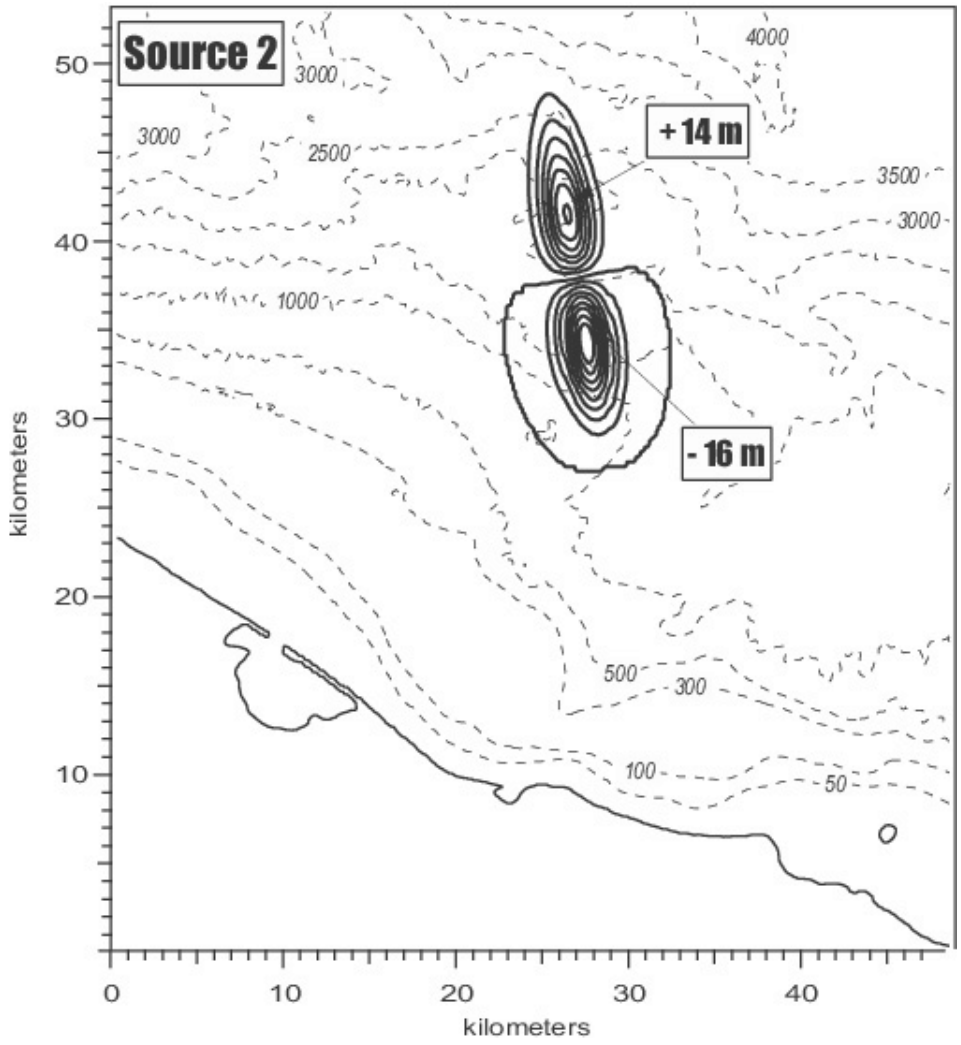

Figure 8
The long-narrow initial condition (LNIC) for the Papua New Guinea event. The island is located on the bottom of the figure; Sissano Lagoon is shown.

the deeper water, near the source, there is virtually no difference between the models. As the wave approaches the spit, the scenario changes, and NLSW predicts a considerably larger wave, nearly 10 m higher. Interestingly, there is a sharp contrast between the large difference between the models and a much smaller difference as the wave travels shoreward. This contrast is attributed to wave breaking, in fact, it occurs in the same region where breaking is initiated in both the models. The nearshore cancellation of the large differences in the models just seaward of the

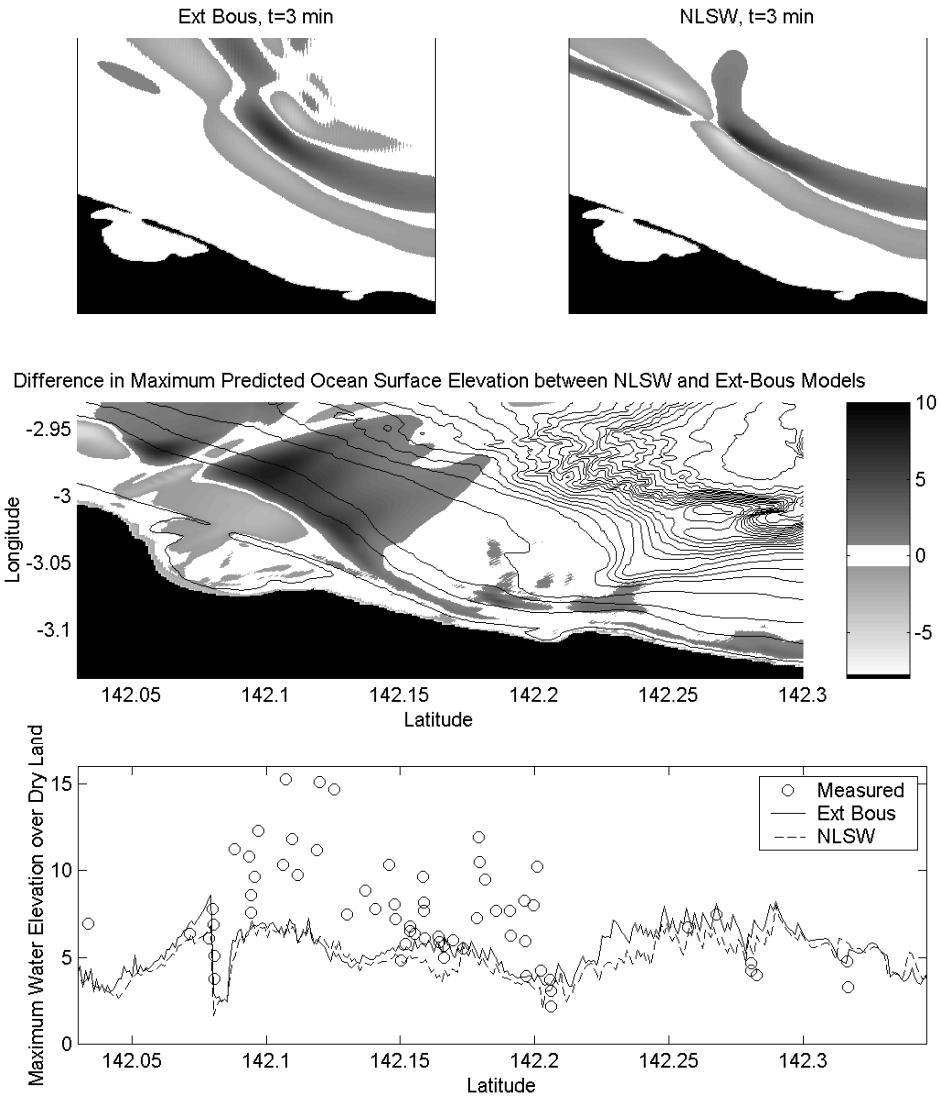

Figure 9

Dispersion effects with the long-narrow initial condition. The top plots (in the top row) show the instantaneous free surface elevation predicted by the NLSW and BOUS models. The middle plot shows the difference in maximum free surface elevation between the models. Positive values indicate that the shallow water model predicts a higher free surface at that location. The lower plot compares the predicted inland water elevations with field data.

breaking line is a strong indication that breaking in this area is depth-limited. The lower plot in the figure shows the maximum free surface elevation predicted over dry land, including over the inundated spit. Also plotted are the recorded field data. The BOUS and NLSW predict very similar flooding patterns, although there exist local

differences on the order of 40%, particularly east of latitude 142.15. It may be possible that east of this latitude, breaking is not governed by depth, whereas seaward of the spit, breaking is depth-limited.

Numerical results for the second initial condition, SFIC, are shown in Figure 10. All of the conclusions stated in the above paragraph, for LNIC, are directly applicable to initial condition SPIC as well. Some differences do exist however. Examining the middle plot in Figure 10, we see that the region of largest difference between the NLSW and BOUS models is shifted to the east, as compared to the same plot in Figure 9. This is due to the fact that with SFIC, wave energy is focused slightly more to the east than with LNIC, and where the largest waves are located will also be the location of the largest difference between the NLSW and BOUS models. The numerical results using SFIC appear to give a better agreement than LNIC with the field data for water elevation over dry land.

Thus far, only the spatial differences due to dispersive effects have been examined. It would likewise be interesting to look at the time-dependent aspects, such as differences in tsunami arrival time, and number of crests. To do this, time series of the numerical free surface elevation are recorded at three different locations. The three locations are located near the shoreline, and are given in Figure 11. The time series comparisons at these three locations are shown in Figure 12 for the SFIC. Clearly, BOUS and NLSW predict very different waveforms. In all of the plots in Figure 12, the BOUS model gives a first crest arrival time roughly 30 seconds later than the NLSW model. This time corresponds to the arrival time of the second trough in the NLSW results. The number of distinct wave crests contained in the waveform is the same with both models. While it is immediately evident that frequency dispersion has a leading order impact on the wave form, it is equally clear that this impact would be difficult to extract from eyewitness accounts. An eyewitness arrival time record with an accuracy of seconds would be a tough find, especially in the PNG area.

It would seem that for the PNG case, in the region of primary interest (near the lagoon), frequency dispersion effects are unimportant to the prediction of runup and inundation. This is not because dispersion effects are unimportant offshore, it is only because of what appears to be depth-limited breaking negating a large difference in offshore wave height. While use of NLSW might lead to good runup prediction, other properties of the tsunami, such as wave shape and arrival time, show larger errors. It should be noted, however, that the large uncertainty associated with the tsunami generation dynamics in the source region represents an error much larger than that due to neglect of frequency dispersion.

3.2.1 Sensitivity of predicted PNG runup to initial condition

In the previous section, two initial conditions, LNIC and SFIC, were discussed. In this section, the relation between these two initial conditions will be more closely scrutinized, along with a third initial condition. This third initial condition, meant to

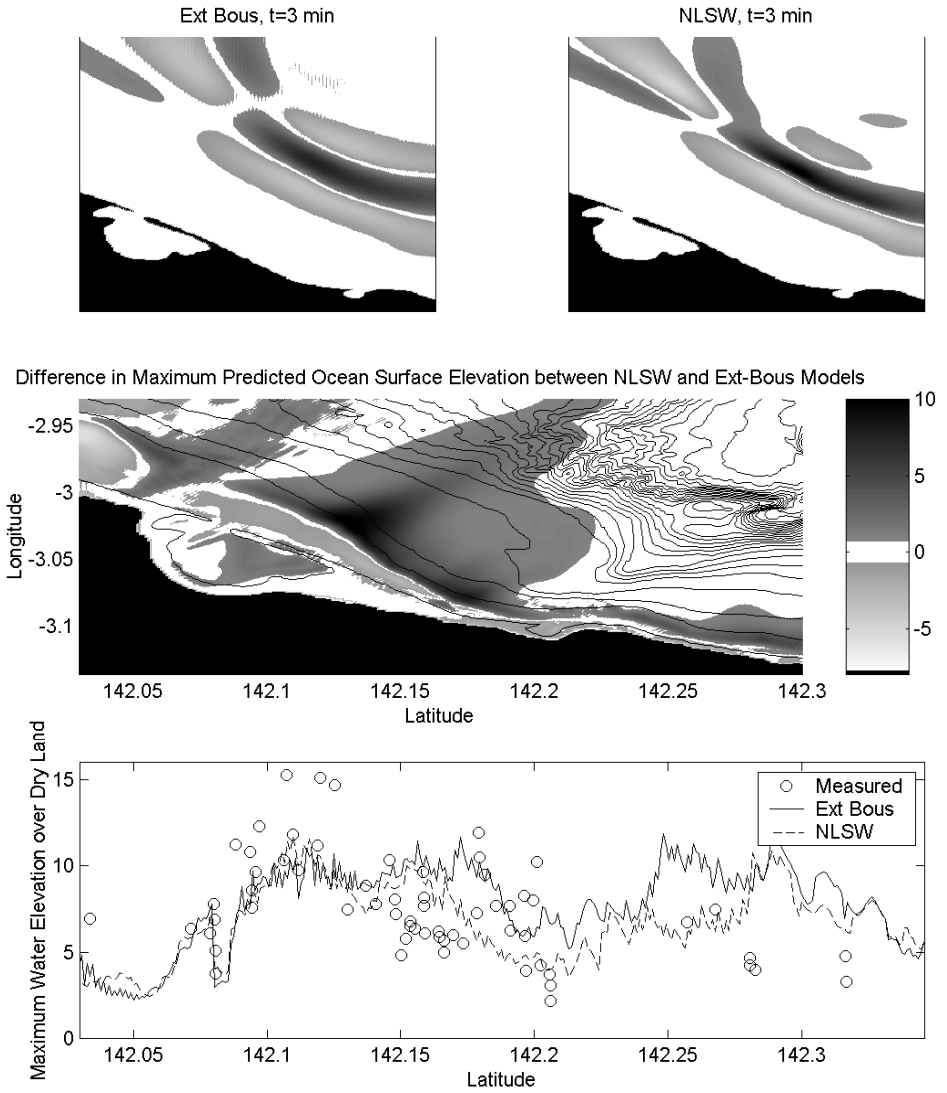

Figure 10

Dispersion effects with the short-fat initial condition. The top plots (in the top row) show the instantaneous free surface elevation predicted by the NLSW and BOUS models. The middle plot shows the difference in maximum free surface elevation between the models. Positive values indicate that the shallow water model predicts a higher free surface at that location. The lower plot compares the predicted inland water elevations with field data.

be close to the simplest reduction to the complex hot start problem, is a single sine wave fit with a Gaussian distribution in the transverse direction. The sine wave has a length of 10 km and a width of 5 km. The sine wave initial condition, or SineIC, is centered at the same location as the other two initial conditions.

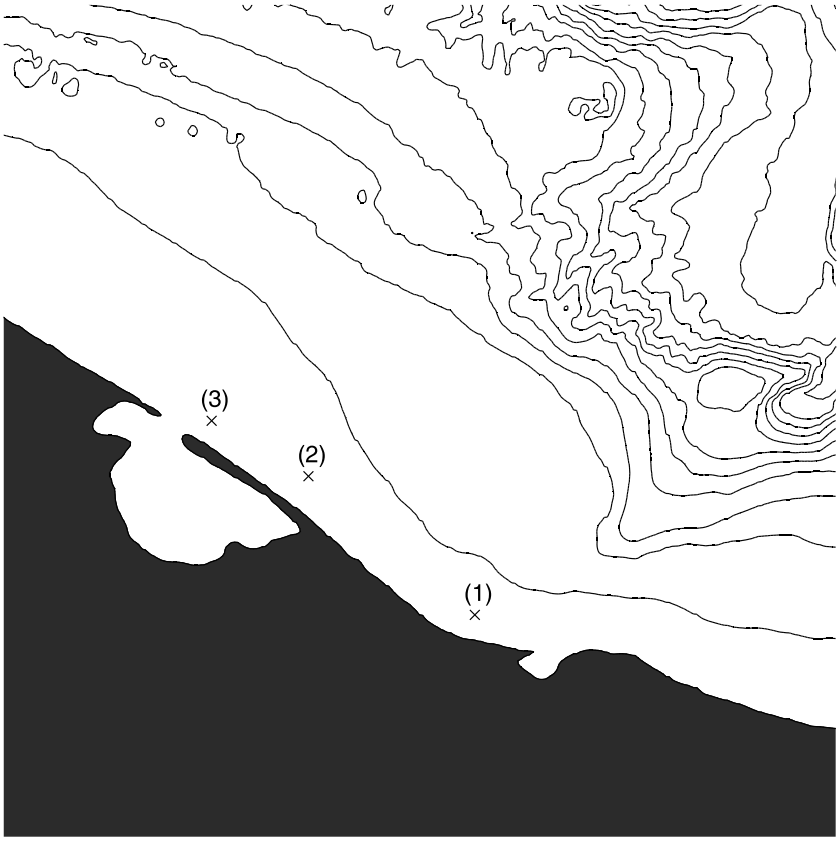

Figure 11
Locations of the PNG time series comparisons. Depth contours are every 100 m.

Figure 13 shows a number of snapshots of the free surface for all three initial conditions. In the first column are the numerical results, using BOUS, with SFIC, the second column with LNIC, and the third column SineIC. The first row are the initial conditions, at time = 0. The second row, at time = 1 minute, shows the three initial conditions spreading out radially. At time = 3 minutes, shown in the third row, it is clear how the different initial conditions each produce very different offshore wave heights and different number of waves. In the last row, at time = 7 minutes, breaking has initiated in all of the simulations, creating similar wave heights offshore of the lagoon for all three initial conditions, but still different number of waves.

A summary of the numerical results from the three initial conditions is given in Figure 14. In the top row are shown the maximum free surface elevations predicted by the three initial conditions. SFIC gives the largest maximum free surface elevation, and also predicts the highest flooding of dry land, as shown by the lower plot. LNIC and SineIC are in close agreement overall.

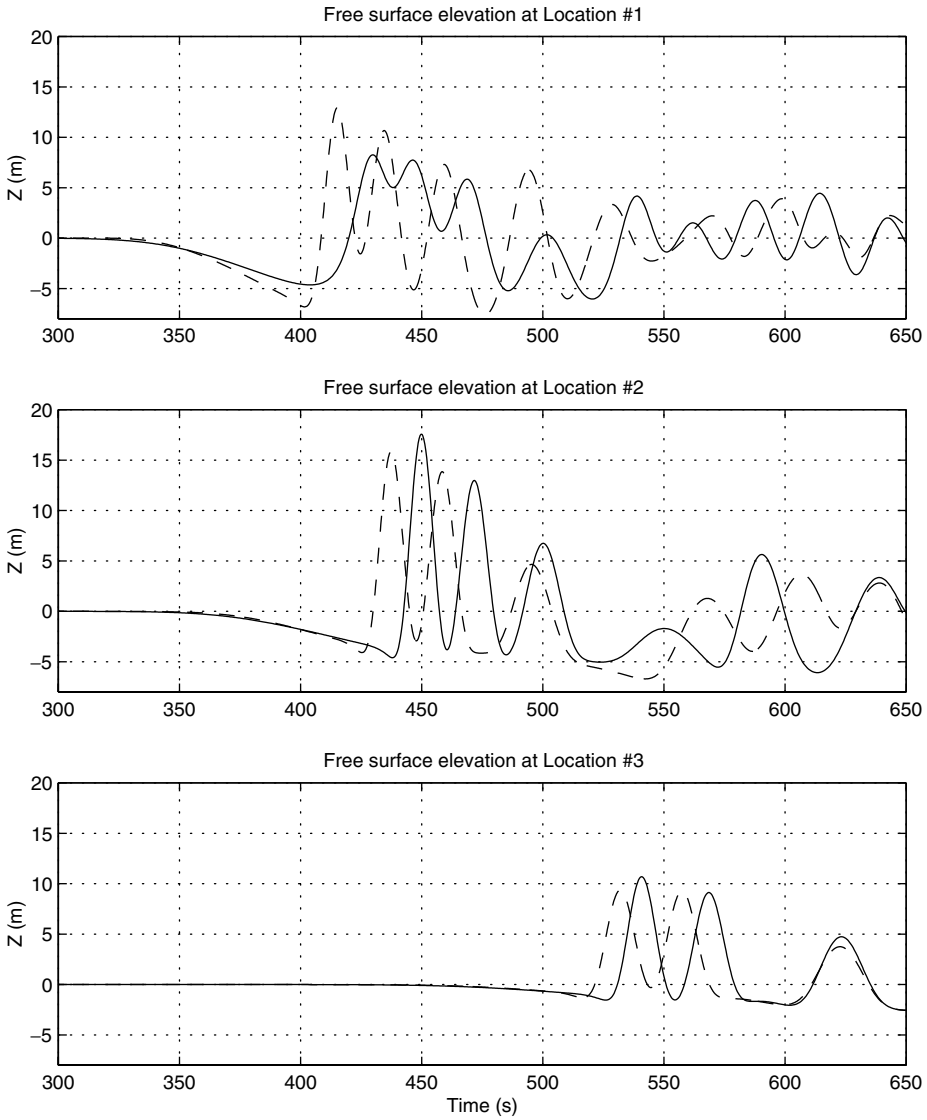

Figure 12
PNG time series comparisons of the free surface for the three locations shown in Figure 11, for the SFIC. BOUS results are given by the solid line, NLSW by the dashed line.

Let us now examine the maximum predicted free surface elevation averaged over the spit (roughly 142.09 to 142.2 degrees). Over this distance, the SFIC predicts heights in the range of 10 meters. The LNIC and the SineIC predict nearly the exact inundation patterns, with an average height near 6 meters. It is interesting to note that despite the large difference in shape between LNIC and SineIC, the

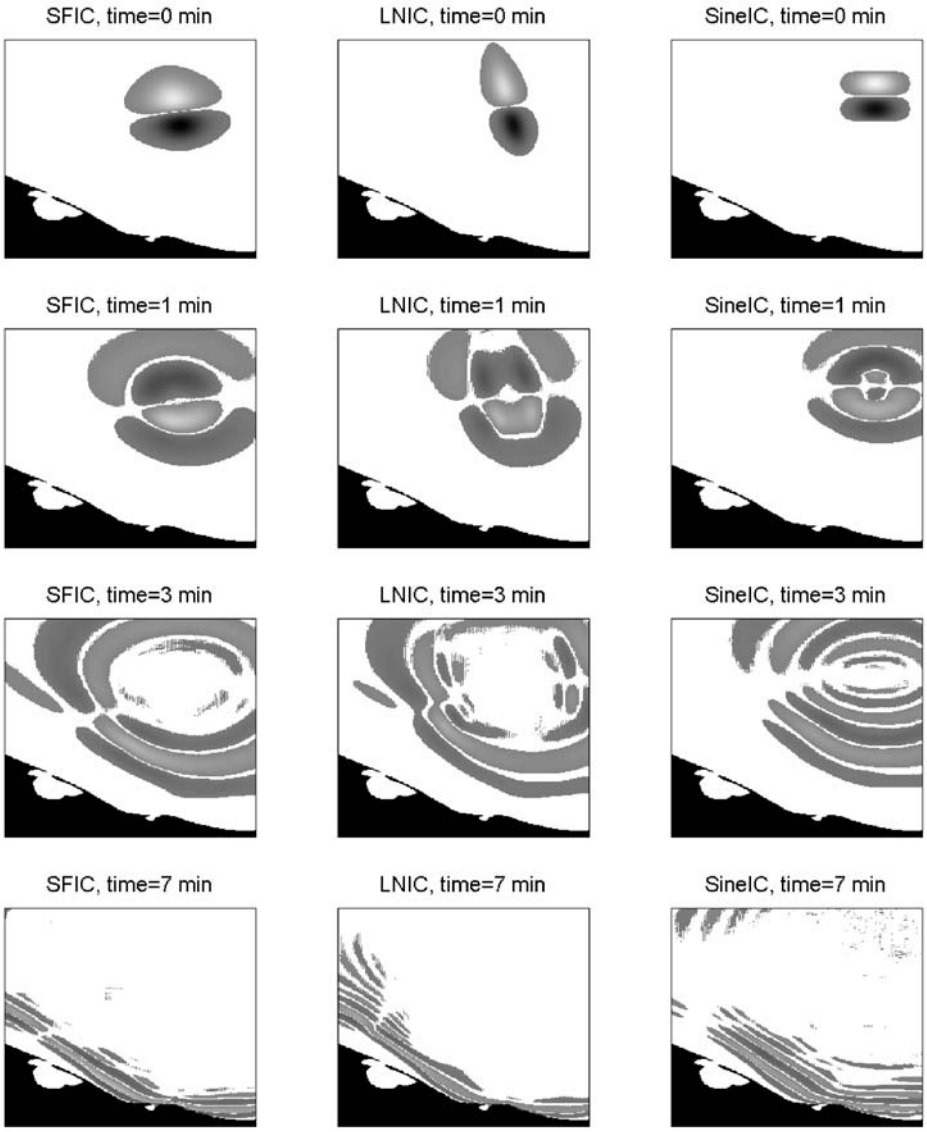

Figure 13
The evolution in time of three different initial conditions. In the first column are the results from the short-fat initial condition, the middle column the long-narrow initial condition, and the last column the sine-wave initial condition. The first row is for the initial time, the second row for $t = 1$ min, the third for $t = 3$ min, and the fourth for $t = 7$ min.

predicted runup are in good agreement. One possible explanation for this agreement is that the displaced water mass of the initial condition is the dominant factor in predicting runup for this case, whereas the shape and orientation will play

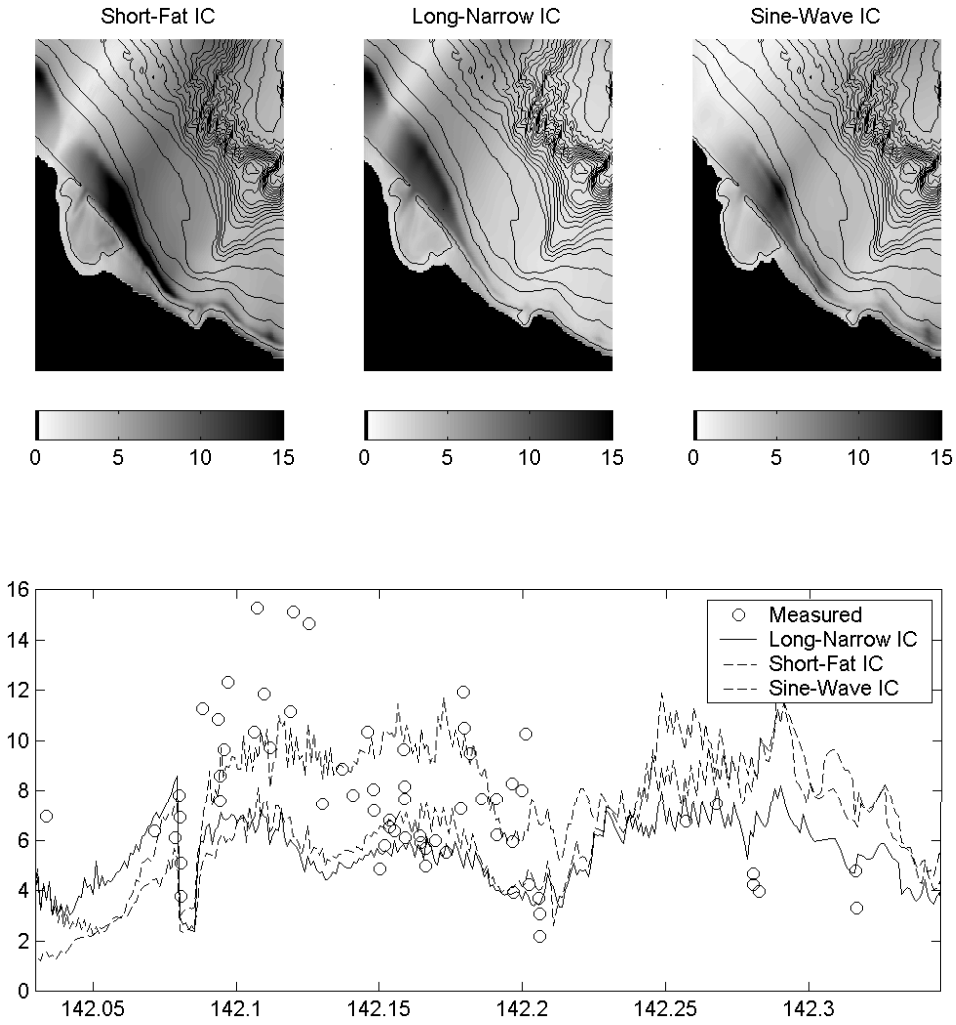

Figure 14
Comparisons from the three different initial conditions. The top row shows the maximum ocean surface predicted by the different initial conditions, and the bottom plot compares the inland free surface elevations.

secondary roles. The initial displaced mass, or the displaced mass of the "hot start" condition, is given by:

$$M = \rho \int_0^L \int_0^W |\zeta(x, y, t = 0)| \, dx \, dy \tag{7}$$

where L and W are the domain widths in the y and x directions and ρ is the density of water. The following ratios are calculated:

$$\frac{M(\text{LNIC})}{M(\text{SFIC})} = \frac{M(\text{SineIC})}{M(\text{SFIC})} = 0.58. \tag{8}$$

Note that the maximum depression of SineIC was chosen so that its initial M was equal to that of LNIC. Not coincidentally, the ratios of M are very close to the ratios of maximum inundation heights over the spit (6 m/10 m). Thus, it would seem that the finer detail of the initial condition plays a small role in maximum runup for the PNG case. However, these details will play a significant role in the prediction of wave arrival time, the maximum runup away from the spit, and the number of distinct waves hitting the coastline.

3.2.2 Interpretation of numerical output with respect to the measured field data

While the numerical model employed in the previous section is capable of simulating the tsunami overtopping of the Sissano spit, many other frequently used tsunami models are not. Presently, most published and validated tsunami inundation models compute either the largest inundation height over dry land, whether runup or inundation depth (MOST) or a water surface elevation at the first offshore wet point (TSUNAMI-N2) or water elevation at an offshore threshold depth (e.g., YEH *et al.*, 1996). In the case of a low relief topography where overtopping is possible, unless care is taken in the computation, models may output as "runup" what is really computed flow depth over the existing topography (see Fig. 15). In order to actually compute runup in Sissano, the model must compute evolution of the breaking wave over the spit, into and across the lagoon, and finally into mangroves and palm forest. Breaking wave computations are chancy at best with the tried shallow water wave models, and the propagation of a broken wave over extreme shallow water can be unstable as well.

The tsunami propagation and inundation model used in this section solves the NLSW equations in characteristic form. The runup code uses a moving boundary

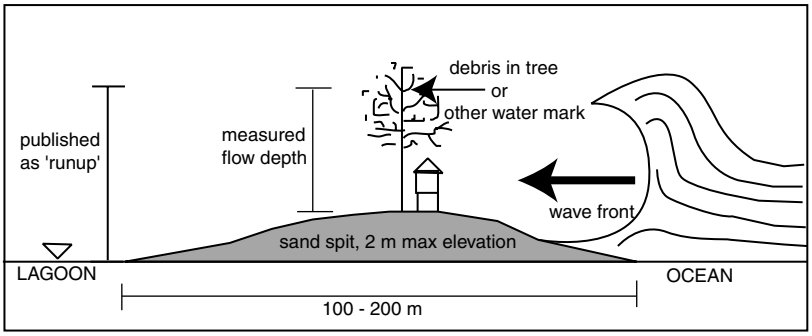

Figure 15
A cartoon showing the difference between measured flow depths and published runup in the case of the Papua New Guinea tsunami.

algorithm that extends the computational domain as needed for the flow conditions. The particular version used is known by the acronym MOST (TITOV and GONZALEZ, 1997), and is currently used at the University of Southern California and at NOAA's Pacific Marine Environmental Laboratory. It has been validated repeatedly through comparison with laboratory data and comparisons with field measured tsunami runup data (TITOV and SYNOLAKIS, 1995, 1997, 1998).

To test the effect of the sand spit at Sissano Lagoon on the model results, two different simulations were run. One with the existing topography and bathymetry, and another with a 1:30 slope along the entire shore, including the lagoon. A 1:30 slope is used because it is close to the existing slope. An initial grid spacing of approximately 140 m was used. Note that the numerical model used (MOST) develops a variable spaced grid from the input bathymetry. In these cases, the near shore and overland grid spacing was approximately 80 m.

The initial wave used in these simulations is the SFIC. The results from the two cases are shown in Figure 16. The shoreline shown in the runup figures is that of the undisturbed real shoreline. In the upper panel, the concentric black contour lines are the contours of the initial surface displacement. In the lower panel, the solid lines show the computed runup using the existing topography. MOST calculates the largest inundation height over dry land, whether runup or flow depth. In the case of a uniformly sloping beach, maximum runup is the highest inundation height. In the case of the model with the Sissano spit the highest inundation height is over the spit. Note how the runup values drop off in the region of the narrow sand spit. The dashed lines show the computed runup in the case of a uniform plane beach. The computed runup values along the sand spit are considerably higher and closer to what was reportedly measured in the field. They are also consistent with laboratory data on solitary waves, which suggest that the maximum runup is up to twice larger than the flow depth at the initial shoreline.

As discussed earlier, the field measurements taken along the Sissano sand spit are subject to considerable uncertainty. Are the measured values representative of the flow depths, or are they local maxima? Were the watermarks really caused by this event? Is it possible that the flow conditions were so extreme that local extrema could be generated by splash that cannot yet be calculated adequately by the models? Even casual observers of breaking long waves in real beaches would notice that the splash spray exceeds the maximum height of the wave.

To address this question, a series of numerical wave gages was placed along the eastern spit (Figure 17). Superimposed on Figure 17 is the maximum computed water elevation (bars) and the field measured flow depths (crosses and circles). To make the measurements compatible with the computational results, the height of the local topography was subtracted from the measured value. If the height of the local topography was not measured, a nominal 2 m, the maximum recorded elevation over the spit, was subtracted. Adjusting these values and comparing it to a computed flow depth brings the results of the numerical simulation in better agreement with the

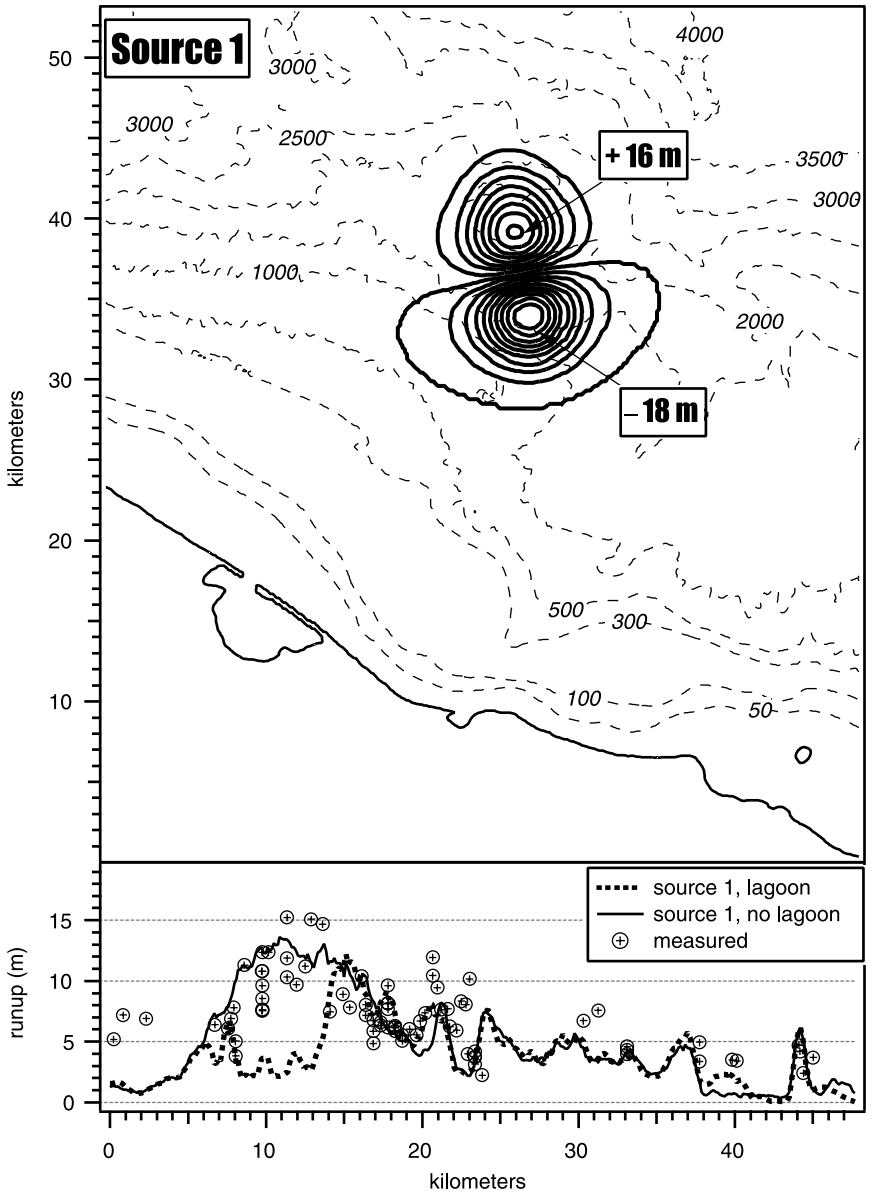

Figure 16

Upper panel – the offshore bathymetry and contours of the initial wave shape (thick black contours). Lower panel, computed runup for cases with existing topography including the lagoon and with a 1:30 plane beach along the entire shore. The spike on the right side of the figure refers to runup on Tumleo Island off Aitape. Measured runup there was 4.5 m.

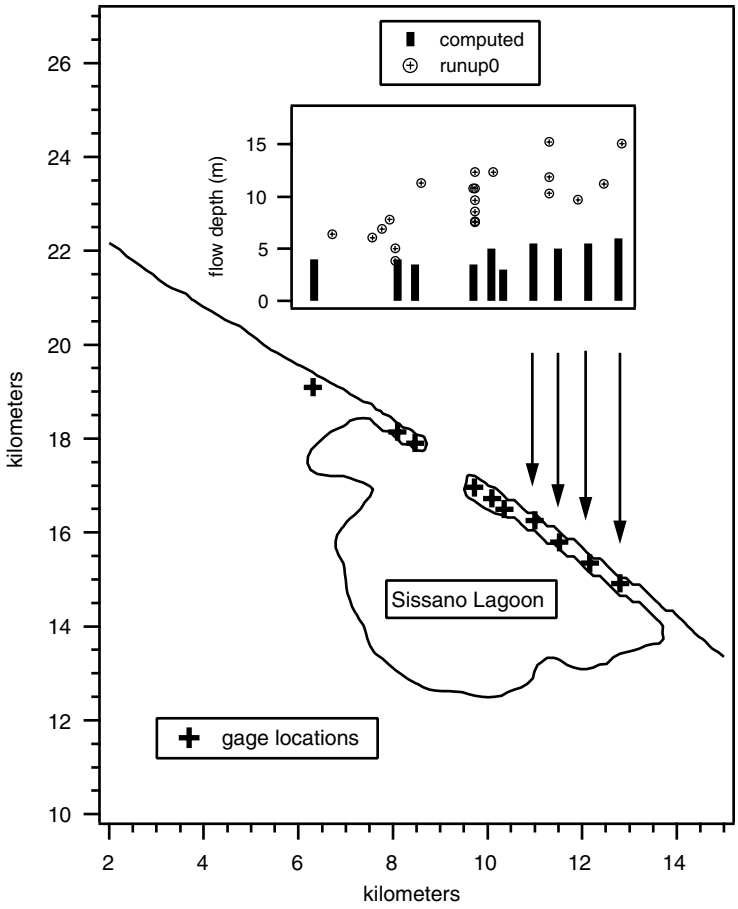

Figure 17
A close-up of the Sissano Lagoon region showing the locations of numerical wave gages (crosses) and the corresponding computed flow depths (black bars). Plotted above the black bars are the measured data converted to a flow depth above the ground surface (circles with cross).

field-measured data, however errors of 50% are evident. For comparison, purely tectonic sources do not produce significant overtopping of the spit (SYNOLAKIS *et al.*, 2002).

Due to the problems with the field data recorded after the 1998 tsunami survey, it is proposed here that a new runup plot be considered when discussing the Papua New Guinea tsunami. In this new runup plot, the points that are ''true'' runup values will be kept the same while points collected along the sand spit or in other areas where a true runup reading could not be attained will be differentiated and noted as ''measured flow depths.''

An example of this revised runup plot is shown in Figure 18.

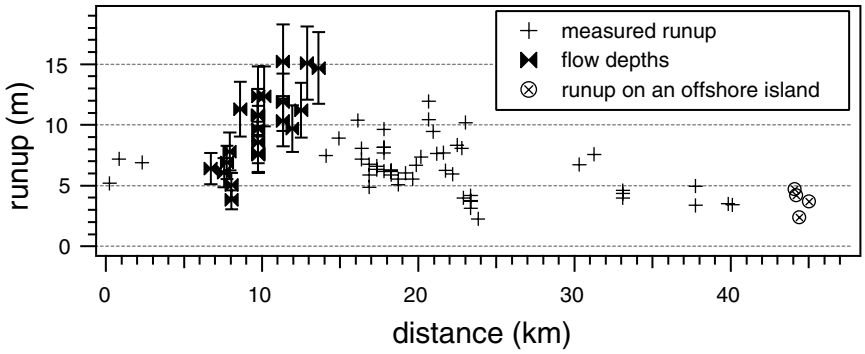

Figure 18
A proposed alternate version of the Papua New Guinea runup plot, with the values around Sissano Lagoon differentiated as 'flow depths' and plotted with 20% error bars.

4. Conclusion

The Papua New Guinea tsunami was a brutal display of the power of nature and a catalyst for a paradigm shift within the tsunami research community. As this shift occurs, the applicability of using traditional dislocation source tsunami propagation codes for landslide tsunamis must be checked. Landslides represent a different type of source, creating waves with different general characteristics. Landslides tsunamis, as demonstrated by the PNG wave, can have lengthscales too small to be accurately modeled with nondispersive models. Offshore wave elevation predictions of the Boussinesq and NLSW models differ by as much as 10 meters where the Boussinesq model predicts a height of 5 meters. However, due to bathymetry effects, namely depth-limited breaking, the inundation due to the PNG tsunami can be accurately simulated with a NLSW model near the spit. This effect is site-specific to PNG, and therefore the good runup prediction of NLSW models for this event cannot be used as justification to apply a NLSW model to a future landslide tsunami occurrence.

The breaking effects offshore of the spit must also be considered when justifying an initial condition for the PNG tsunami. As shown in this paper, unique initial conditions do not lead to unique maximum sea-surface elevation patterns over the spit. In fact, it was shown that the water elevations over the spit are far more closely related to the magnitude of the displaced mass contained in the initial condition. This is not true away from the spit, though, where the breaking appears not to be depth-limited. Finally, given the behavior of numerical bores in well-used tsunami codes, it is recommended that computations with current inundation tools which model evolution over narrow spits be bracketed between two runup distributions, one over a uniform beach and one over the spit.

Acknowledgements

The research reported here is partially supported by Grants from National Science Foundation (CMS 9908392 and CMS 0217744).

References

Chen, Y. and Liu, P. L.-F. (1995), *Modified Boussinesq Equations and Associated Parabolic Model for Water Wave Propagation*, J. Fluid Mech. *228*, 351–381.

Kawata, Y., Benson, B., Borrero, J. C., Davies, H. L., deLange, W. P., Imamura, F., Letz, H., Nott, J., and Synolakis, C. E. (1999), *Tsunami in Papua New Guinea was as Intense as First Thought*, EOS, Transact. Am. Geophys. Union *80*(9), 101, 104–105.

Kennedy, A. B., Chen, Q., Kirby, J. T., and Dalrymple, R. A. (2000), *Boussinesq Modeling of Wave Transformation, Breaking, and Runup. Part I: 1D*, J. Waterway, Port, Coastal and Ocean Eng. 126(1), 39–47.

Lynett, P., Wu, T.-R., and Liu, P. L.-F. (2002), *Modeling Wave Runup with Depth-Integrated Equations*, Coast. Eng. 46(2), 89–107.

Lynett, P. and Liu, P. L.-F. (2002), *A Numerical Study of Submarine Landslide Generated Waves and Runup*, Roy. Soc. London A, *485* (2028), 2885–2910.

Nwogu, O. (1993), *Alternative Form of Boussinesq Equations for Nearshore Wave Propagation*, J. Waterway, Port, Coastal and Ocean Eng. *119*(6), 618–638.

Okal, E. (2003), *Normal Mode Energetics for Far-field Tsunamis Generated by Dislocations and Landslides*, Pure Appl. Geophys. *160*, 2189–2221.

Press, W. H., Flannery, B. P., and Teukolsky, S. A., *Numerical Recipes*. (Cambridge University Press 1989), pp. 569–572.

Synolakis, C. E., Bardet, J.-P., Borrero, J. C., Davies, H. L., Okal, E. A., Solver, E. A., Sweet, S., and Tappin, D. R. (2002), *The Slump Origin of the 1998 Papua New Guinea Tsunami*, Roy. Soc. London A *458*, 763–789.

Tappin, D. R. *et al*. (1999), Sediment Slump Likely Caused 1998 Papua New Guinea Tsunami. EOS *80*(30), 329.

Titov, V. and Gonzalez, F. (1997), *Implementation and Testing of the Method of Splitting Tsunami (MOST) Model*, NOAA Technical Memorandum ERL PMEL – 112.

Titov, V. V. and Synolakis, C. E. (1995), *Modeling of Breaking and Nonbreaking Long Wave Evolution and Runup Using VTCS-2,* J. Waterway, Port, Coastal and Ocean Eng. *121*, 308–316.

Titov, V. V. and Synolakis, C. E. (1997), *Extreme Inundation Flows during the Hokkaido-Nansei-Oki Tsunami*, Geophys. Res. Lett. *24*, 1315–1318.

Titov, V. V. and Synolakis, C. E. (1998), *Numerical Modeling of Tidal Wave Runup*, J. Waterway, Port, Coastal and Ocean Eng. *124*(4), 157–171.

Yeh, H., Liu, P. L.-F., and Synolakis, C. eds (1996), *Long-wave Runup Models*, Proc. 2nd Int. Workshop on Long-wave Runup Models, World Scientific Publishing Co., Singapore.

Zelt, J. A. (1991), *The Runup of Nonbreaking and Breaking Solitary Waves*, Coast. Eng. *15*, 205–246.